Study of acoustic resonance in enclosures using eigenanalysis based on boundary element methods

Mingsian R. Bai

Department of Mechanical Engineering, National Chaio Tung University, 1001 Ta Hsueh Road, Hsin Chu 30050, Taiwan, Republic of China

It is well known that, from the modal theory of room acoustics, resonance will occur if the driving frequency of a sound source located in a room coincides with one of the natural frequencies of the sound field. In this study, an eigenanalysis technique based on the boundary element method (BEM) is developed for extracting eigenmodes of a sound field in an enclosure. A method of singular value search, in conjunction with a golden section optimization algorithm, is utilized for efficient calculation of eigenmodes. In particular, modes associated with repeated eigenvalues can be well resolved by the technique developed in this research. Enclosures of various geometries have been analyzed by using the developed algorithm in a numerical simulation. Satisfactory agreement has been achieved between the BEM results, the FEM results, and the analytical solutions if available.

INTRODUCTION

Resonance phenomenon in an enclosure is one of the important subjects in research of acoustics. The importance lies in the fact that the knowledge of acoustic eigenmodes is essential to the analysis of dynamic responses of a sound field in an enclosure. For example, modal theory is employed in room acoustics for analyzing reverberation phenomena when ray acoustics does not provide, especially for low and intermediate frequency ranges, a complete modeling of sound fields in an enclosure.[1,2] Adequate distribution of resonance frequencies and mode shapes is very critical in the optimal design of a room. Another example is the knock phenomenon of combustion chambers. Research[3] has shown that combustion knock, which is harmful to engines, is mainly due to acoustic resonance in combustion chambers. Proper tuning of resonance frequencies will reduce combustion knock to a minimum so that engine performance can be improved.

While separable coordinate systems[4] are available for analytically calculating acoustic eigenmodes in dealing with enclosures of simple geometries, one has to resort to numerical methods, e.g., the finite element method (FEM) and the boundary element method (BEM) for enclosures of complex geometries. Since only boundary meshes need be constructed in the application of BEM, dimensionality of the original problem is reduced by one. This fact makes BEM a particularly attractive technique for eigenanalysis of enclosure resonance.

The objective of this study is to develop a numerical technique for extracting acoustic eigenmodes in enclosures based on the boundary element formulation and to demonstrate how best to implement it. Problems involved in the implementation phase including resolution of eigenmodes associated with repeated eigenvalues and algorithms of efficient search for eigenmodes are investigated. In order to verify the BEM-based eigenanalysis technique, a rectangular room with a known exact solution is selected as the first test

object in a numerical simulation. Numerical performance of the developed method is also compared with that of another commonly used method, FEM. Higher accuracy has been achieved by using BEM than FEM. Then, both methods are applied to the case of a car interior. The results of eigenmodes obtained from these eigenanalysis methods display excellent agreement.

I. THE BEM-BASED EIGENANALYSIS TECHNIQUE

In the beginning of this section, the theory of integral equations for the boundary value problems of sound fields will be briefly reviewed. Then, a BEM-based eigenanalysis technique in conjunction with eigenmode search schemes will be presented. Some technical problems during the implementation phase will also be discussed.

A. The BEM-based eigenanalysis of sound field in an enclosure

From the theory of linear acoustics, it is well known that the solution of a boundary value problem (see Fig. 1) associated with a monochromatic sound field in an enclosure is represented by the following Kirchhoff–Helmholtz equation:[4-6]

$$\alpha p(\mathbf{x}_p) = \int_S G(\mathbf{x}_p, \mathbf{x}_q) \frac{\partial p}{\partial n}(\mathbf{x}_q)$$

$$- p(\mathbf{x}_q) \frac{\partial G}{\partial n}(\mathbf{x}_p, \mathbf{x}_q) dS_q, \tag{1}$$

where

$$\alpha = \begin{cases} 1, & \mathbf{x}_p \in V \\ 0, & \mathbf{x}_p \notin (V \cup S) \\ \frac{1}{2}, & \mathbf{x}_p \in S, \quad S \text{ a smooth surface} \\ \Omega/4\pi, & \mathbf{x}_p \in S, \quad S \text{ a nonsmooth surface} \\ & (\Omega \text{ is the solid angle}).[5] \end{cases}$$

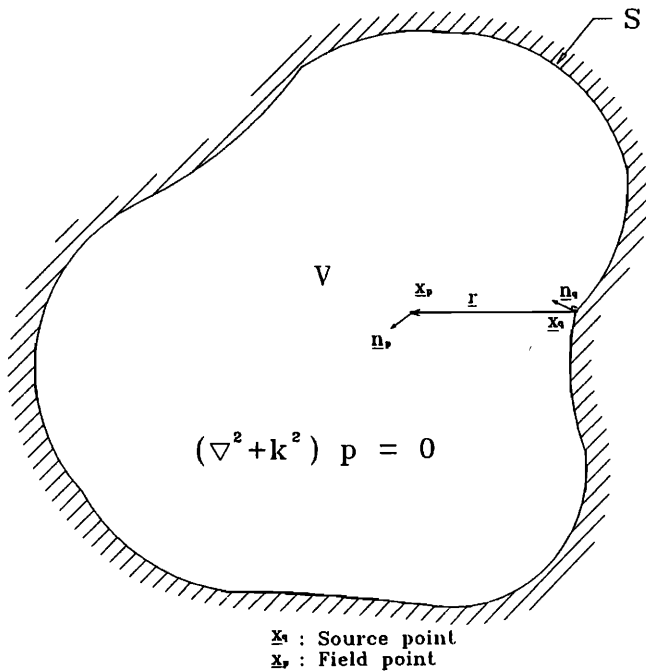The complex variable $p(\mathbf{x})$ denotes the sound pressure mea-

$(\nabla^2 + k^2) \, p = 0$

V

$\underline{x}_q$: Source point
$\underline{x}_p$: Field point

FIG. 1. Schematic diagram for the interior boundary value problem of a sound field in an enclosure.

sured at the location **x**. The free-space Green's function $G(\mathbf{x}_p,\mathbf{x}_q) = \exp(ikr)/4\pi r$ for the Helmholtz equation in a three-dimensional space. The parameter k is the wave number ($k = \omega/c$, with ω being the angular frequency and c being the speed of sound). The position vector $\mathbf{x}_p$ and $\mathbf{x}_q$ denote, respectively, the field point and the source point. The distance $r = |\mathbf{x}_p - \mathbf{x}_q|$. The directional directive $\partial/\partial n \equiv \mathbf{n}\cdot\nabla$ with **n** being the outward normal to the surface S.

On the basis of boundary integral equations, we are now in a position to develop a BEM-based technique for the eigenanalysis of a sound field in an enclosure. In this study, triangular elements and quadrilateral elements are used to construct a mesh on a surface. Isoparametric transformation is adopted for discretizing a boundary. The same set of quadratic shape functions are used to interpolate global coordinates, sound pressures, and pressure gradients on a boundary as follows:[7]

$$x_i(\xi) = \sum_{l=1}^{L} N_l(\xi) x_{il}, \quad i = 1,2,3; \; L = 6 \text{ or } 8, \tag{2}$$

$$p_m(\xi) = \sum_{l=1}^{L} N_l(\xi) p_{ml}, \quad m = 1,2,...,M; \; L = 6 \text{ or } 8, \tag{3}$$

$$\frac{\partial p_m}{\partial n_q}(\xi) = \sum_{l=1}^{L} N_l(\xi) \frac{\partial p_{ml}}{\partial n_q}, \quad m = 1,2,...,M; \; L = 6 \text{ or } 8, \tag{4}$$

where x_{il} is the ith coordinate of the lth node, $N_l(\xi)$ are the quadratic shape functions, $\xi \equiv (\xi_1,\xi_2)$ are the local coordinates, p_{ml} and $\partial p_{ml}/\partial n_q$ are the sound pressure and the pressure gradient of the lth node on the mth element, and M is the total number of elements. Substituting Eqs. (2)–(4) and

$$\frac{\partial G}{\partial n_q} = \mathbf{n}_q(\xi)\cdot\nabla G(\mathbf{x}_p,\mathbf{x}_q(\xi))$$

into Eq. (1) gives the following discretized boundary integral equation:

$$\alpha_i p(\mathbf{x}_p)$$
$$= \sum_{m=1}^{M} \left\{ \left[\int_{S_m} G(\mathbf{x}_p,\mathbf{x}_q(\xi)) |\mathbf{J}(\xi)| \mathbf{N}(\xi) dS_q \right] (\mathbf{p}_n)_m] \right.$$
$$\left. - \left[\int_{S_m} \nabla G(\mathbf{x}_p,\mathbf{x}_q(\xi))\cdot\mathbf{n}_q(\xi) |\mathbf{J}(\xi)| \mathbf{N}(\xi) dS_q \right] \mathbf{p}_m \right\}, \tag{5}$$

where α_i is the solid angle parameter of the field point $\mathbf{x}_p$, ∇G is the gradient of G, S_m is the surface of the mth element, $\mathbf{J}(\xi)$ is the Jacobian for coordinate transformation, $\mathbf{p}_m$ and $(\mathbf{p}_n)_m$ are $L \times 1$ column vectors corresponding, respectively, to p_{ml} and $\partial p_{ml}/\partial n_q$ terms in the integral equations, and $\mathbf{N}(\xi)$ is an $1 \times L$ row vector with $N_l(\xi)$ as its components. In terms of operator notation, Eq. (5) can be assembled into the following matrix form for a mesh with M elements and N nodes on the boundary:

$$\alpha_i p(\mathbf{x}_p) = \mathbf{S}^{pq}\mathbf{p}_n^q - \mathbf{D}^{pq}\mathbf{p}^q, \tag{6}$$

where $\mathbf{p}^q$ and $\mathbf{p}_n^q$ are $N \times 1$ row vectors corresponding to the sound pressure $p(\mathbf{x}_q)$ and the pressure gradient $\partial p(\mathbf{x}_q)/\partial n_q$, respectively, of the N nodes $\mathbf{x}_q$, and $\mathbf{S}^{pq}$ and $\mathbf{D}^{pq}$ are both $1 \times N$ row vectors corresponding to the integrals in the square brackets of Eq. (5). The superscript pq denotes the spatial transformation from the field point $\mathbf{x}_p$ to the source points $\mathbf{x}_q$.

Now, taking the field points to the boundary S and setting $\alpha_i = \frac{1}{2}$ or $\Omega_i/4\pi$ (Ω_i denotes the solid angle at the field point $\mathbf{x}_p$ and $i = 1,2,...,N$), depending on whether the surface is smooth or not, one obtains

$$\alpha\mathbf{p}^q = \mathbf{S}^{qq}\mathbf{p}_n^q - \mathbf{D}^{qq}\mathbf{p}^q \tag{7}$$

or

$$\bar{\mathbf{D}}\mathbf{p}^q = \mathbf{S}^{qq}\mathbf{p}_n^q, \tag{8}$$

where α is an $N \times N$ diagonal matrix whose diagonal terms are composed of the parameters α_i's corresponding to the N nodes on the boundary. $\mathbf{D}^{qq}$ and $\mathbf{S}^{qq}$ are both $N \times N$ square matrices corresponding to the integrals in Eq. (5) relating the N field points $\mathbf{x}_p$ and the N source points $\mathbf{x}_q$ on the boundary S, the superscript qq signifies that both the field points and source points are colocated on the boundary S, and $\bar{\mathbf{D}} \equiv (\mathbf{D}^{qq} + \alpha)$.

In some situations, care should be taken for the treatment of nonsmooth surfaces. Recall that the parameter α_i in Eq. (5) equals $\frac{1}{2}$ for smooth surfaces and $\Omega_i/4\pi$ for nonsmooth surfaces. It usually poses difficulties in direct evaluation of the solid angle Ω_i. This difficulty can be circumvented by applying a uniform potential to the interior domain to yield[7]

$$\alpha_d = -\int_{S_m} \nabla G(\mathbf{x}_p,\mathbf{x}_q(\xi))\cdot\mathbf{n}_q(\xi) |\mathbf{J}|\mathbf{N} \, dS_q]^{pq}\mathbf{u}$$

or

$$\alpha_i = -\sum_{j=1}^{L} (\mathbf{D}^{qq})_{ij}, \tag{9}$$

where α_d is an $N \times 1$ column vector that is composed of α_i's,

u denotes an $N \times 1$ column vector whose terms are all ones, and $(\mathbf{D}^{qq})_{ij}$ are the components of $\mathbf{D}^{qq}$.

In this study, the walls of enclosures are assumed to be rigid, which is approximately true in many cases, e.g., a hard-walled room. This corresponds to imposing the boundary condition $\partial p/\partial n = 0$ on S. Thus, Eq. (8) is simply reduced into

$$\overline{\mathbf{D}}\mathbf{p} = 0. \tag{10}$$

Here, Eq. (10) constitutes the main equation of the BEM-based eigenanalysis of a sound field in an enclosure. In principle, the wave numbers k's that render the matrix $\overline{\mathbf{D}}$ singular should be the desired eigenvalues. The eigenvectors associated with each eigenvalue can be obtained from finding the nontrivial solutions of Eq. (10). Nevertheless, care should be taken because Eq. (10) is not the usual form of the generalized eigenvalue problem $\mathbf{A}\mathbf{x} = \lambda \mathbf{B}\mathbf{x}$ and accordingly must be handled differently. In the case of the BEM-based formulation discussed herein, the eigenvalues are embedded in the kernel functions G or $\partial G/\partial n$ and the coefficient matrix $\overline{\mathbf{D}}$ is a function of the eigenparameter λ. This peculiarity of the BEM-based formulation precludes the use of standard eigensystem solvers such as those widely used in the FEM. Therefore, special eigenmodes search schemes, e.g., the method of determinant search and the method of singular value search, are developed in this study to alleviate this numerical difficulty.

B. The search schemes for eigenmodes

In the method of determinant search, one seeks to determine the eigenvalues by incrementally varying the wave number k such that the matrix $\overline{\mathbf{D}}$ in Eq. (10) becomes singular.[8,9] This amounts to finding the wave numbers k_e, $e = 1,2,...$, so that the determinant of $\overline{\mathbf{D}}$ vanishes. In numerical implementation, however, one can only search local minima of the determinant of $\overline{\mathbf{D}}$ for the eigenvalues because it is virtually impossible for $\overline{\mathbf{D}}$ to become ideally singular except for some special cases.[10] Once the eigenvalue k_e's have been found, the natural frequency ω_e's can readily be recovered from $\omega_e = k_e c$.

In addition to eigenvalues k_e's, the eigenvectors $\mathbf{p}_e$'s remain to be found. The eigenvector $\mathbf{p}_e$, which represents the eigenmode associated with the eigenvalue ω_e, is, by definition, the nontrivial solution of the following equation:

$$\overline{\mathbf{D}}_e \mathbf{p}_e = 0, \tag{11}$$

where the $N \times N$ matrix $\overline{\mathbf{D}}_e$ is obtained from the coefficient matrix $\overline{\mathbf{D}}$ evaluated at $k = k_e$ and the eigenvector $\mathbf{p}_e$ is an $N \times 1$ column vector. These nontrivial solutions of Eq. (11) can be calculated by the Gauss elimination algorithm.

In addition to the previously mentioned determinant search method, another approach based on singular value decomposition (SVD) is developed in this study for calculating eigenmodes. From the theory of linear algebra, the following decomposition of an arbitrary matrix $\overline{\mathbf{D}}$ is always possible:[11]

$$\overline{\mathbf{D}} = \mathbf{U}\mathbf{\Sigma}\mathbf{V}^h, \tag{12}$$

where h is the Hermitian conjugate operator, $\mathbf{U}$ and $\mathbf{V}$ are

both $N \times N$ unitary matrices and are composed of N orthogonal column vectors $\mathbf{u}_i$'s and $\mathbf{v}_i$'s, respectively, and $\mathbf{\Sigma}$ is a pseudodiagonal matrix (but is a diagonal matrix in our case):

$$\mathbf{\Sigma}_{ij} = \begin{cases} \sigma_i \geqslant 0, & i = j \\ 0, & i \neq j \end{cases}$$

(σ_i's are singular values arranged in descending order). If the matrix $\overline{\mathbf{D}}$ is almost singular, then the rank of $\overline{\mathbf{D}}$ tends to be degenerate with the last one or more singular values being nearly negligible in comparison with the rest of singular values. In the initial stage of extracting the eigenvalues k_e's, the coefficient matrix $\overline{\mathbf{D}}$ is evaluated with the wave number k incrementally varied by a coarse step size Δk. In each iteration, the matrix $\overline{\mathbf{D}}$ associated with different k is processed by the SVD algorithm. The minimal singular value obtained at the rth iteration (denoted by $\sigma_{n,r}$) is compared with the minimal singular values σ_n's obtained from the other iterations. If $\sigma_{n,r}$ is smaller than those obtained from the adjacent iterations, i.e., $\sigma_{n,r-1}$ and $\sigma_{n,r+1}$, then at least one eigenvalue must exist within the interval $(k - \Delta k, k + \Delta k)$.

Having established a search interval for an eigenmode, one may proceed to calculate a more accurate value of a particular mode. Instead of using a sequential search procedure, a more efficient optimization technique termed the "golden section search algorithm"[12] is then utilized for locating the eigenvalue of interest. This simple search method is selected because the gradient of the cost function (which is difficult to estimate in our case) is not required. In general it takes less than 10 search step to reach accuracy within two decimal places.

Parallel to searching for eigenvalues, the eigenvectors are obtained from the SVD process without additional effort. This is manifested by postmultiplying Eq. (12) by $(\mathbf{V}^h)^{-1}$:

$$\overline{\mathbf{D}}(\mathbf{V}^h)^{-1} = \mathbf{U}\mathbf{\Sigma}$$

or

$$\mathbf{D}\mathbf{V} = \mathbf{U}\mathbf{\Sigma} \tag{13}$$

since $\mathbf{V}^h = \mathbf{V}^{-1}$ from the property of unitary matrices. Further partitioning of Eq. (13) yields

$$\mathbf{D}\mathbf{v}_i = \sigma_i\mathbf{u}_i. \tag{14}$$

Whenever the singular value $\sigma_i = 0$, Eq. (14) becomes

$$\mathbf{D}\mathbf{v}_i = 0. \tag{15}$$

Direct comparison of Eqs. (10) and (15) reveals that the eigenvector $\mathbf{v}_i$ in the latter equation is a legitimate nontrivial solution of $\mathbf{D}\mathbf{p} = 0$. In other words, whenever σ_i vanishes, the right singular vector $\mathbf{v}_i$ of $\mathbf{D}$ can be regarded as an eigenvector associated with the eigenvalue k_e.

In addition, this SVD approach for finding eigenvectors is particularly useful when the eigenvalue problem of concern involves nondegenerate repeated eigenvalues (which are frequently encountered in the cases of enclosures with high degree of symmetry). For instance, if the eigenvalue k_e is of multiplicity m, then the last m singular values $\sigma_{n-m+1}, \sigma_{n-m+2},...,\sigma_n$ will be significantly smaller than the others. The orthogonal vectors $\mathbf{v}_{n-m+1}, \mathbf{v}_{n-m+2},...,\mathbf{v}_n$

are accordingly the desired linearly independent eigenmodes associated with the same eigenvalue k_e. In this regard, the method of singular value search has more preferable performance than the method of determinant search because the latter approach fails to provide linearly independent eigenvectors for the cases involving repeated eigenvalues. Thus, in the following sections, the method of singular value search is selected in the BEM-based eigenanalysis for calculating eigenmodes of sound field in an enclosure.

II. VERIFICATION OF THE BEM-BASED EIGENANALYSIS ALGORITHM

In order to investigate numerical characteristics of the developed BEM-based eigenanalysis technique, computer simulations are conducted for extracting eigenmodes of a sound field in an enclosure. The BEM result is compared with the corresponding analytical solution. For a case where the analytical solutions is not available, FEM is selected as an alternative numerical approach. The formulation of the FEM-based eigenanalysis is omitted here because it is quite standard and can be found in the literture.[13-16]

The first simulation case involves determination of eigenmodes of a rectangular room. Consider a rectangular room bounded by rigid walls lying along the planes $x = 0$, $x = L_x, y = 0, y = L_y, z = 0, z = L_z$, as shown in Fig. 2(a). The boundary value problem can be expressed in terms of rectangular coordinates as

$$\frac{\partial^2 p}{\partial x^2} + \frac{\partial^2 p}{\partial y^2} + \frac{\partial^2 p}{\partial z^2} + k^2 p = 0 \qquad (16)$$

subject to $\partial p / \partial n = 0$ on the walls. It can be shown[4] that the
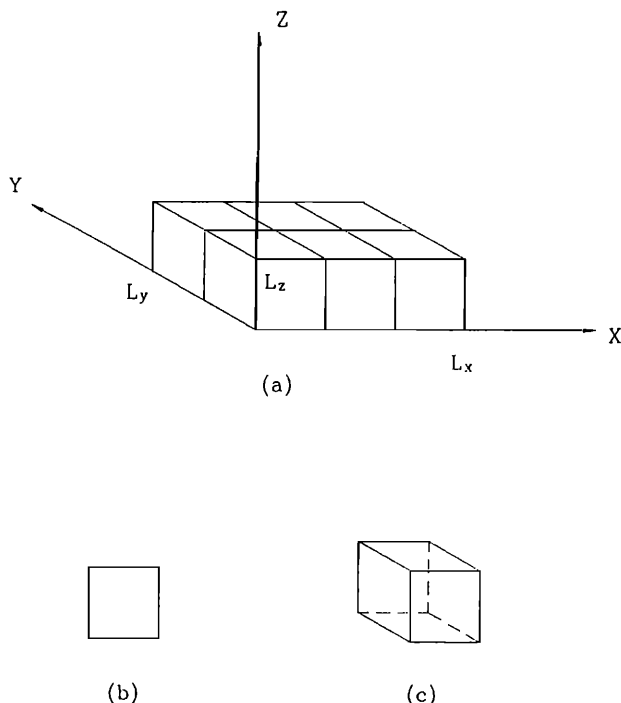
eigenvalues of the above boundary value problem are

$$k(n_x, n_y, n_z) = \pi \sqrt{\left(\frac{n_x}{L_x}\right)^2 + \left(\frac{n_y}{L_y}\right)^2 + \left(\frac{n_z}{L_z}\right)^2} \qquad (17)$$

with the associated eigenfunctions

$$p(x, n_x, n_y, n_z) = A \cos \frac{n_x \pi x}{L_x} \cos \frac{n_y \pi y}{L_y} \cos \frac{n_z \pi z}{L_z}, \qquad (18)$$

where A is an arbitrary constant. Here, an eigenmode is identified by a particular combination of integers n_x, n_y, and n_z. Each of these three integers is assumed nonnegative to avoid redundancy. In this simulation, a rectangular room bounded by rigid walls of dimensions $L_x = 3$ m, $L_y = 2$ m, and $L_z = 1$ m is selected for testing the BEM-based eigenanalysis algorithm.

The results obtained from the BEM-based algorithm are first compared with the corresponding analytical solutions to check if the algorithm is correctly implemented. Since the BEM used for eigenanalysis purpose is a relatively new approach, it is worthwhile to compare its numerical performance with the other methods. To this end, the BEM-based approach is compared with another commonly used numerical method FEM in this simulation. The mesh of BEM coalesce with that of FEM on the boundary in order to achieve a fair comparison. In this case, 22 quadratic rectangular elements with 68 colocation points are used for constructing the BEM mesh, while 6 quadratic brick elements with 70 colocation points are used for constructing the FEM mesh (Fig. 2).

The minimal singular values σ_n's are computed by virtue of the SVD algorithm for different wave numbers k's with initially a coarse step size Δk (0.1 in this case), as shown in Fig. 3. Whenever a local minimum occurs, its adjacent wave numbers are chosen as a search interval for the golden section search algorithm that gives more accurate eigenvalues. In addition to the BEM-based approach, the same case of a rectangular room is analyzed by FEM. The results obtained from both numerical methods are then com-
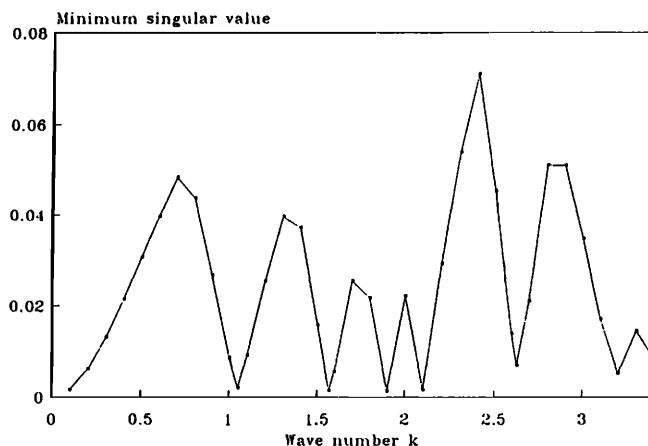

FIG. 2. (a) The mesh for the rectangular room used in the numerical simulation. (b) The boundary element used in the mesh. (c) The finite element used in the mesh.

FIG. 3. The minimum singular values σ_n's calculated for each wave number k in the case of a rectangular room.

TABLE I. Comparison of eigenvalues of the sound field in a rectangular room.

Mode		Eigenvalue k_e			Error (%)	
	(n_x, n_y, n_z)	Exact	BEM	FEM	BEM	FEM
1	(1, 0, 0)	1.05	1.05	1.05	0.00	0.00
2	(0, 1, 0)	1.57	1.57	1.57	0.00	0.00
3	(1, 1, 0)	1.89	1.89	1.89	0.00	0.00
4	(2, 0, 0)	2.09	2.10	2.11	0.48	0.96
5	(2, 1, 0)	2.62	2.63	2.65	0.38	1.14
6	(0, 0, 1)	3.14	3.18	3.46	1.27	10.2
7	(0, 2, 0)	3.14	3.18	3.46	1.27	10.2
8	(3, 0, 0)	3.14	3.18	3.46	1.27	10.2
Average error:		BEM 0.58%				
		FEM 4.09%				

pared with the corresponding analytical solutions in Table I. A sharp contrast of numerical performance is immediately observed from the table. The BEM achieves much higher accuracy (with an average error of eigenvalues 0.58%) than the FEM (with an average error of eigenvalues 4.09%). This could be attributed to the fact that the integral formulation of BEM has well-posed numerical characteristics in comparison with the weak formulation of FEM. Nevertheless, the higher the mode, the larger the error is, regardless of which method is used. In any event, to what extent one is able to search for eigenvalues is basically limited by sound wave length in comparison with the mesh spacing.

Another interesting observation worth mentioning is associated with the last three modes (0, 0, 1), (0, 2, 0), and (3, 0, 0) listed in Table I. These modes correspond to the same eigenvalue 3.14 and are successfully detected by the method of singular value search. The last three singular values computed from decomposing the coefficient matrix $\bar{D}$ evaluated at these repeated eigenvalues 3.14 are closer to zero than the others (see Fig. 4). On the other hand, if there is only one mode associated with some eigenvalue, e.g., $k = 1.05$, only the last singular value will be nearly zero (see Fig. 5).

Some representative eigenmodes obtained from the BEM-based eigenanalysis algorithm are shown in terms of profile curves and 3-D hidden line graphs from Figs. 6–9. Every eigenvector has been normalized with respect to the largest amplitude. Evidently, the calculated eigenmodes appear to agree very well with the exact solutions. In fact, the same BEM technique was also applied to a rigid spherical enclosure. Very good agreement was achieved between the numerical results and the exact solutions. The BEM-based technique again provides much higher accuracy than the FEM-based technique. Since this does not add up any new conclusion, the numerical results are omitted here.

In addition to the previously mentioned rectangular room, a car interior is selected as the second example for testing the usefulness of the BEM-based eigenanalysis technique when applied to a more practical situation where an odd-shaped boundary is present. The motivation of exploring this problem stems from the need of optimizing acoustic performance that could be important for noise control in automobile design.

Consider a car-shaped enclosure with the dimensions as shown in Fig. 10. Since no analytic solution is available for this car interior of complex geometry, comparison of eigenvalues and eigenmodes can only be made between numerical
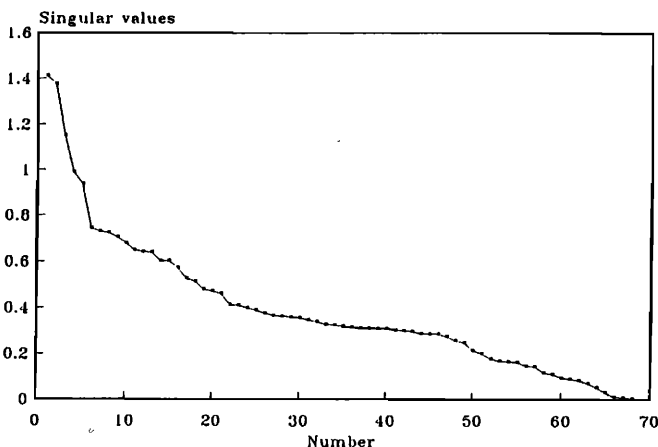

FIG. 4. Singular values associated with the repeated eigenvalue 3.14 corresponding to the modes (0, 0, 1), (0, 2, 0), and (3, 0, 0).
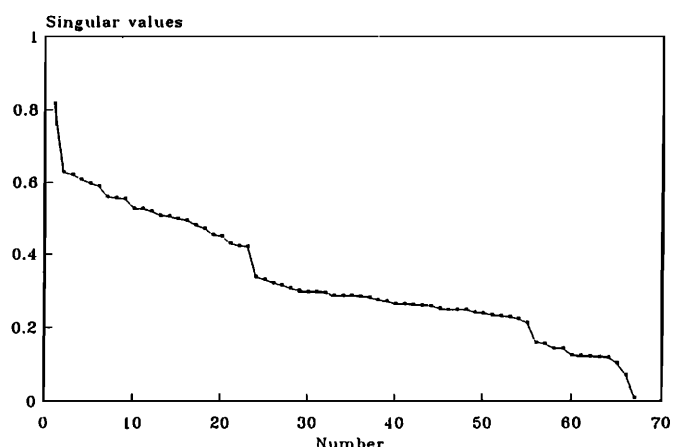

FIG. 5. Singular values associated with the eigenvalue 1.05 corresponding to the single mode (1, 0, 0).
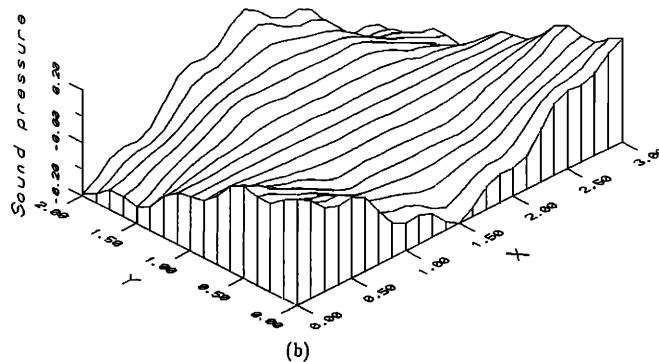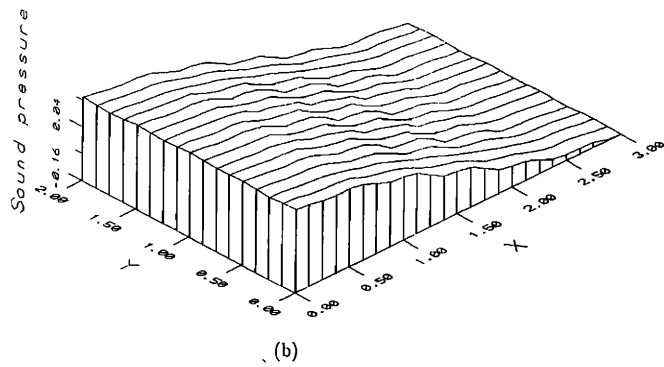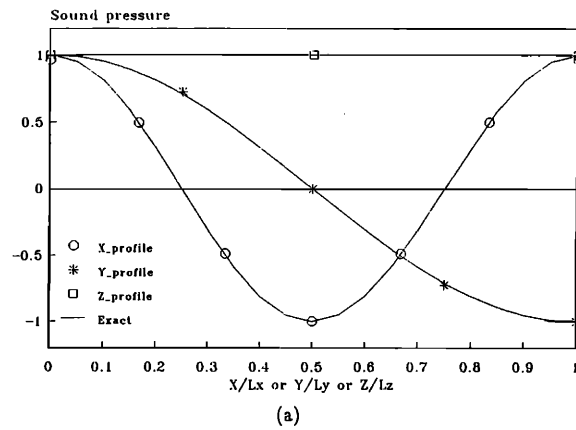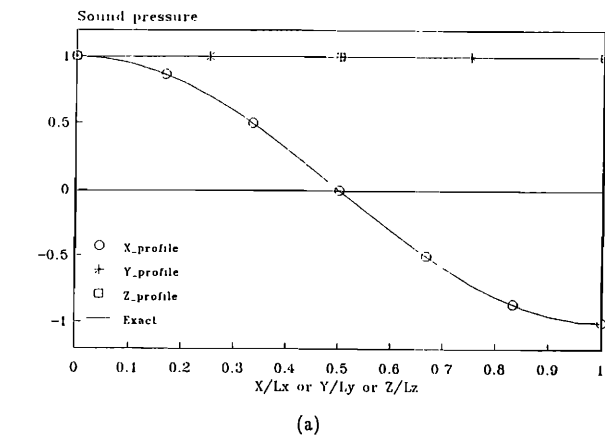
(a)

(b)

FIG. 6. Eigenmode (1, 0, 0) associated with the eigenvalue 1.05 in the case of a rectangular room.

(a)

(b)

FIG. 8. Eigenmode (2, 1, 0) associated with the eigenvalue 2.62 in the case of a rectangular room.
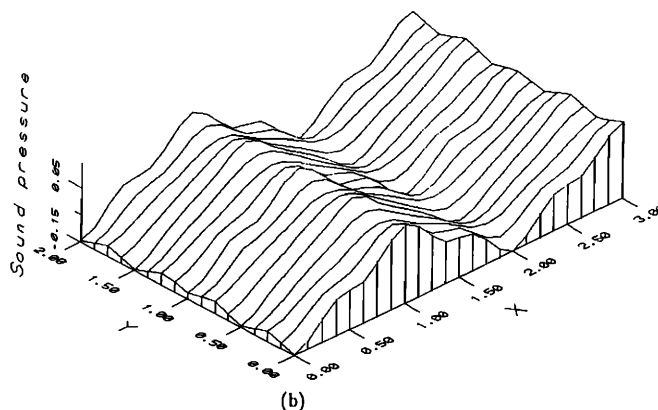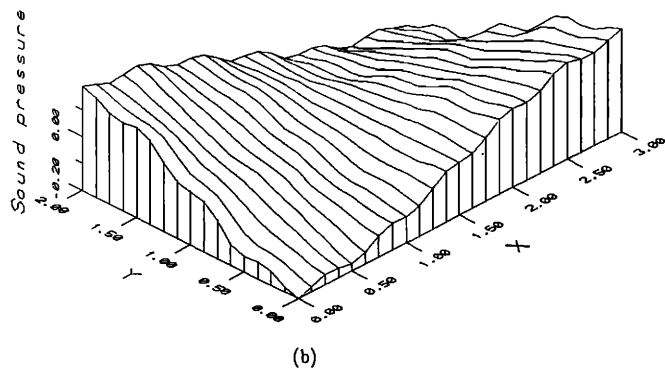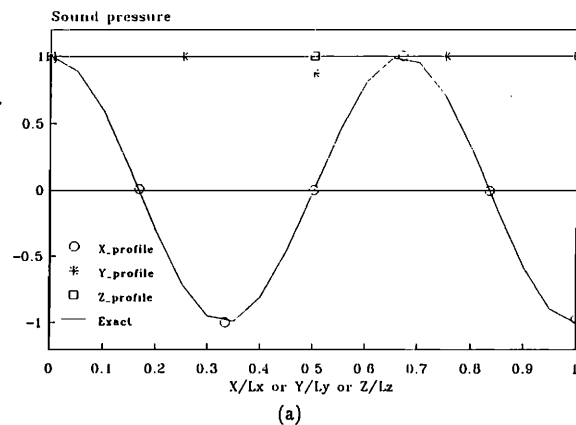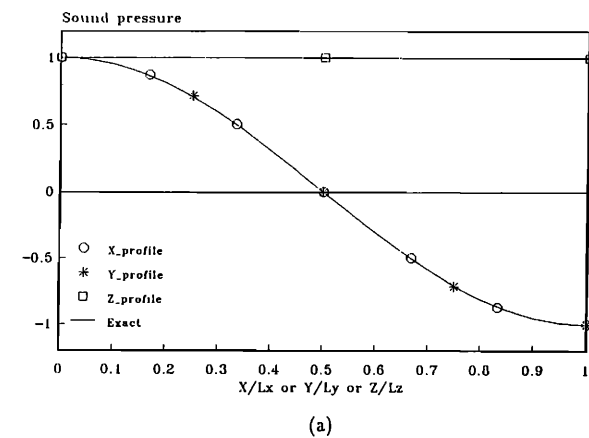

(a)

(b)

FIG. 7. Eigenmode (1, 1, 0) associated with the eigenvalue 1.89 in the case of a rectangular room.

(a)

(b)

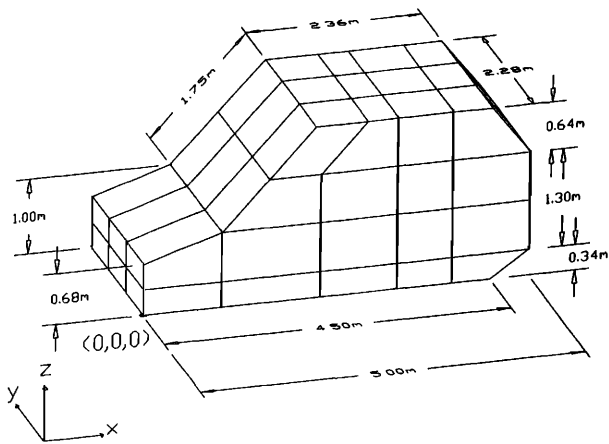FIG. 9. Eigenmode (3, 0, 0) associated with the eigenvalue 3.14 in the case of a rectangular room.

FIG. 10. The mesh and the dimensions of a car interior in the numerical simulation.

methods. In this simulation, the mesh of BEM consists 90 rectangular boundary elements with 272 colocation points and the mesh of the FEM consists of 54 brick elements with 376 colocation points. The problem size is appreciably larger than the case of a rectangular room.

It should be noted that the solid angles at corners and edges of the car interior do not have theoretical values. The numerical technique presented in Sec. I must be utilized to solve for the solid angle parameter α_i associated with each node.

From the simulation results, the BEM-based eigenanalysis technique does exhibit its effectiveness in extracting eigenmodes for an enclosure of complex geometry. In Table II, the eigenvalues of the first five modes obtained from the BEM-based eigenanalysis technique are compared with those obtained from the FEM. Excellent agreement of eigenvalues has been achieved between the BEM and the FEM (the errors are all within 2%). The corresponding eigenmodes are shown in terms of contour graphs from both the side views and the top views (see Figs. 11–15). Differences between the mode shapes obtained from these two numerical methods are barely noticeable. Except for some figures, e.g., Figs. 11(b) and 12(b), which show wavy contours instead of perfect straight lines (due to discretization errors), the mode shapes appear to be satisfactorily computed. No contours appear in Fig. 13(a) and (c) because, for this mode,
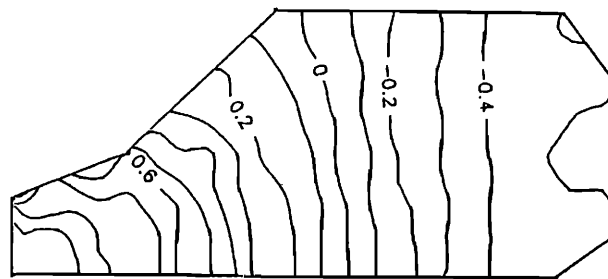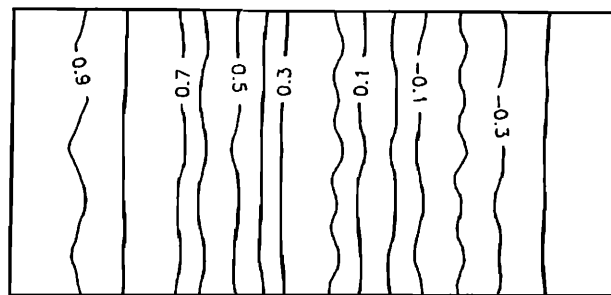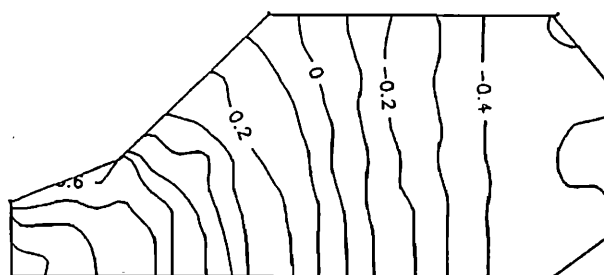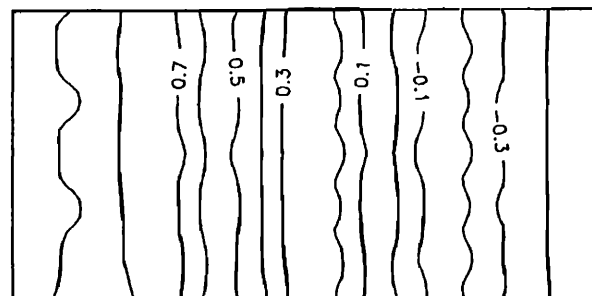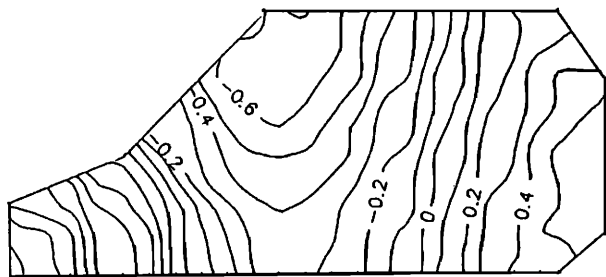

FIG. 11. The first eigenmode of the sound field in the car interior. (a) Pressure contours in plane $y = 0$, obtained from the BEM. (b) Pressure contours in plane $z = 0$, obtained from the BEM. (c) Pressure contours in plane $y = 0$, obtained from the FEM. (d) Pressure contours in plane $z = 0$, obtained from the FEM.

the pressures of all nodes on this plane are supposed to be of a constant level.

Some comments can be made from the computed results in regard to the nature of the mode shapes. Similarities are

TABLE II. Comparison of eigenvalues of the sound field in the car interior.

Mode	Eigenvalue k_e	
	BEM	FEM
1	0.70	0.71
2	1.20	1.22
3	1.40	1.38
4	1.48	1.49
5	1.57	1.55

(a)

(a)

(b)

(b)

(c)

(c)

(d)

(d)

FIG. 12. The second eigenmode of the sound field in the car interior. (a) Pressure contours in plane $y = 0$, obtained from the BEM. (b) Pressure contours in plane $z = 0$, obtained from the BEM. (c) Pressure contours in plane $y = 0$, obtained from the FEM. (d) Pressure contours in plane $z = 0$, obtained from the FEM.

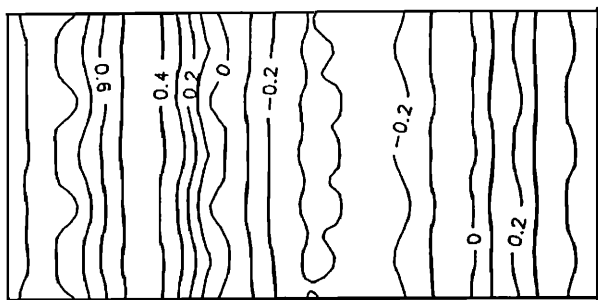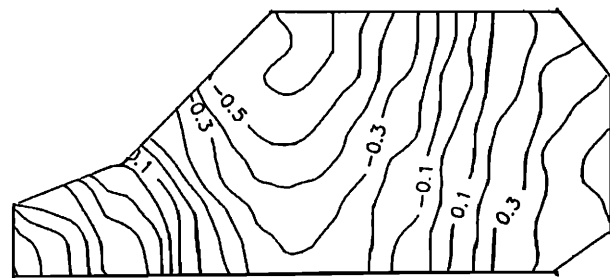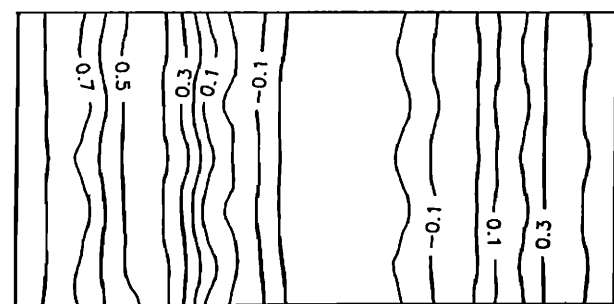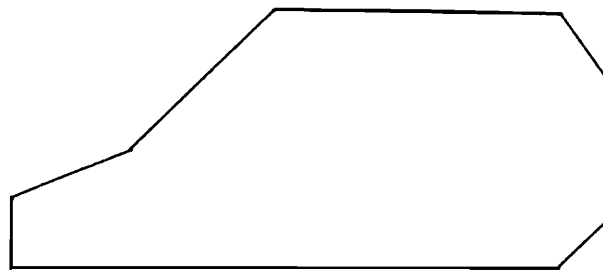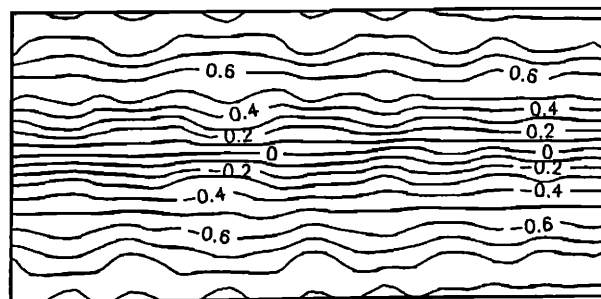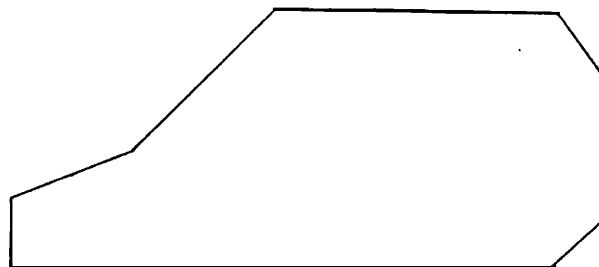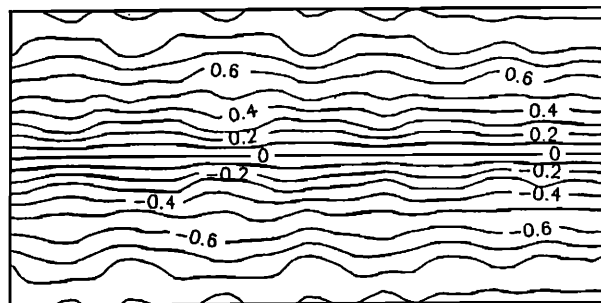FIG. 13. The third eigenmode of the sound field in the car interior. (a) Pressure contours in plane $y = 0$, obtained from the BEM. (b) Pressure contours in plane $z = 0$, obtained from the BEM. (c) Pressure contours in plane $y = 0$, obtained from the FEM. (d) Pressure contours in plane $z = 0$, obtained from the FEM.

found between, for example, Figs. 11(b) and 12(b) as well as Figs. 11(a) and 15(a). This implies these two modes are of identical order in one coordinate surface, but of different order in the others (although these coordinate surfaces al-

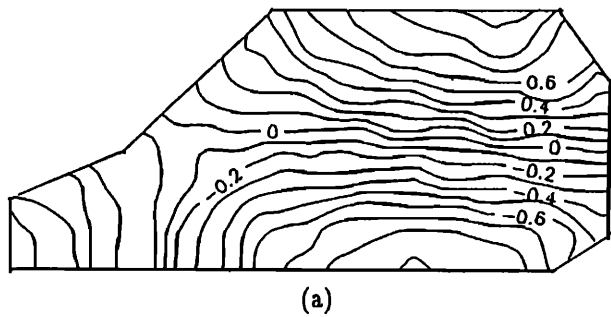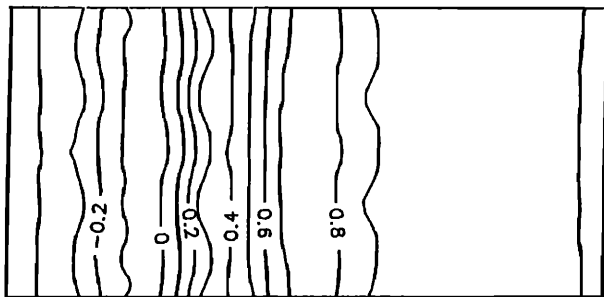ways exist, they do not have analytical forms due to the complex geometry). The higher the resonance frequency is, the more variations there are in the mode shapes, e.g., the symmetric mode in Fig. 11(b) versus the antisymmetric mode in
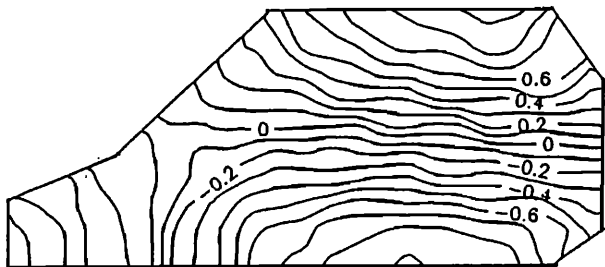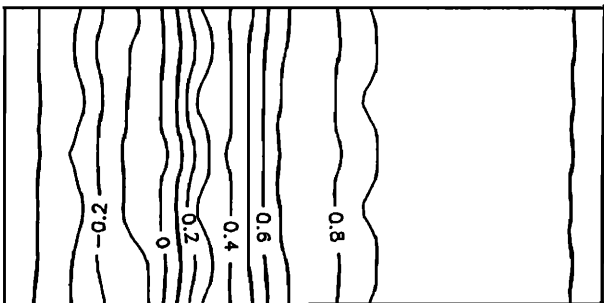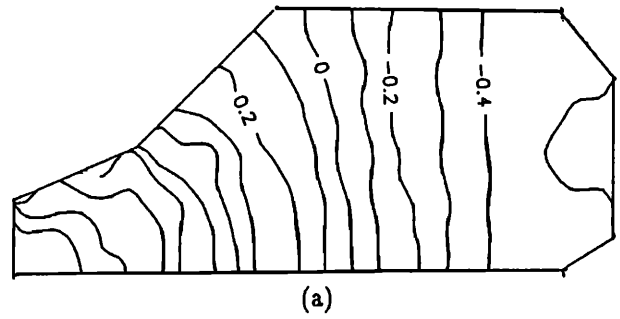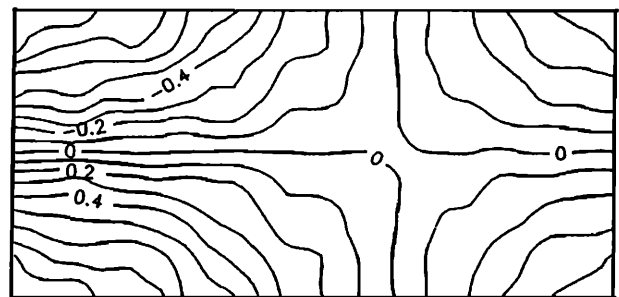
FIG. 14. The fourth eigenmode of the sound field in the car interior. (a) Pressure contours in plane $y = 0$, obtained from the BEM. (b) Pressure contours in plane $z = 0$, obtained from the BEM. (c) Pressure contours in plane $y = 0$, obtained from the FEM. (d) Pressure contours in plane $z = 0$, obtained from the FEM.

FIG. 15. The fifth eigenmode of the sound field in the car interior. (a) Pressure contours in plane $y = 0$, obtained from the BEM. (b) Pressure contours in plane $z = 0$, obtained from the BEM. (c) Pressure contours in plane $y = 0$, obtained from the FEM. (d) Pressure contours in plane $z = 0$, obtained from the FEM.
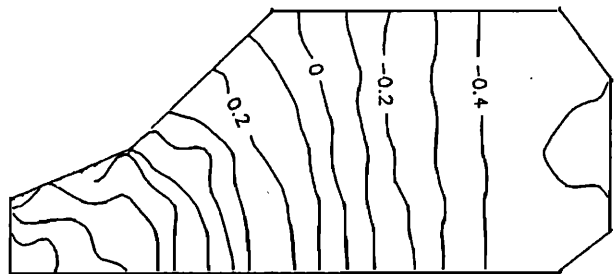
Fig. 15(b). On the other hand, orthogonality is readily observed from some contour figures, e.g., Figs. 11(b) and 13(b). This is a natural consequence of the self-adjoint and undamped eigenvalue problem considered herein.
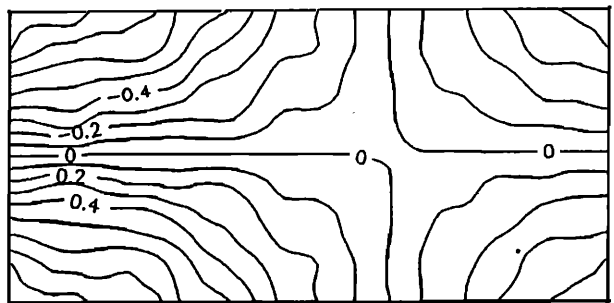
Questions may be raised regarding the use of the eigenmodes associated with a car interior. To the author's knowledge, one possible application is optimizing the acoustical performance for the purpose of noise control. For example,

judging from the pressure distribution in Fig. 15(a), one may want to apply certain sound absorption measures to the regions around the front end as well as the rear part of the car interior where pressure magnitudes reach maxima if the frequency of the major concern is around 38 Hz. In addition, if a hi-fi stereo system is to be installed in the car, one may prefer a relatively uniform distribution, e.g., the pressure field in Fig. 13, of the sound field over a nonuniform one. Under these circumstances, the BEM-based eigenanalysis technique serves as a useful simulation tool for extracting resonance frequencies and mode shapes of sound fields before an actual prototype of a car is built.

III. CONCLUSIONS

A BEM-based eigenanalysis technique is presented in this study for extracting eigenmodes of sound fields in arbitrarily shaped enclosures. Complete procedures involved in numerical implementation are demonstrated in details. The method of singular value search is utilized to determine natural frequencies and mode shapes of sound pressure distribution (associated with not only distinct but also repeated eigenvalues).

The BEM eigenanalysis technique has been verified through comparisons between the numerical results and the exact solution if available. In addition, the BEM results are also compared with those obtained from the FEM in order to explore the numerical performance. The BEM approach, interestingly enough, achieves much higher accuracy than the FEM despite the fact that the errors of the higher modes are always greater than those of the lower ones, regardless of which numerical method is used. It is of no doubt that these numerical schemes will lose their effectiveness at high-frequency ranges due to increasing density of eigenmodes.

The sizes of the resulting system matrices of the BEM are always smaller than those of the FEM because the required meshes for the BEM are simpler than those for the FEM. This should become more pronounced for the enclosures of large volume-to-surface ratio in a three-dimensional space. This reduction of problem size facilitates generation of boundary meshes with reference to the design changes regarding boundary conditions and geometry of an enclosure. This attractive feature makes BEM-based eigenanalysis technique a useful simulation tool before an actual prototype is built. Note that the BEM, while dimensionally smaller than the FEM, takes more CPU time than the FEM

because of full and asymmetric nature of assembled matrices. More research is required for improving the efficiency of the BEM-based approach.

Although the boundaries of enclosures have been assumed perfectly rigid in this study, the BEM-based eigenanalysis technique can be easily extended to the other types of boundary such as the pressure-release type, the impedance type, and the mixed type. These aspects will be explored by more numerical as well as experimental investigations in the future research.

[1] A. D. Pierce, *Acoustics* (McGraw-Hill, New York, 1981).
[2] L. E. Kinsler, A. R. Frey, A. B. Coppens, and J. V. Sanders, *Fundamentals of Acoustics* (Wiley, New York, 1982).
[3] R. Hickling, D. A. Feldmaier, F. H. K. Chen, and J. S. Morel, "Cavity Resonances in Engine Combustion Chambers and Some Applications," J. Acoust. Soc. Am 73, 1170–1178 (1983).
[4] P. M. Morse and K. U. Ingard, *Theoretical Acoustics* (McGraw-Hill, New York, 1968).
[5] G. F. Roach, *Green's Functions* (Cambridge U.P., New York, 1982).
[6] R. E. Kleinman and G. F. Roach, "Boundary Integral Equations for The Three-Dimensional Helmholtz Equation," SIAM Rev. 16, 216–236 (1974).
[7] P. K. Banerjee and R. Butterfield, *Boundary Element Methods in Engineering Science* (McGraw-Hill, New York, 1981).
[8] G. DeMey, "Calculation of the Eigenvalues of Helmholtz Equation by An Integral Equation," Int. J. Num. Meth. Eng. 10, 56–66 (1976).
[9] M. Kitahara, *Boundary Integral Equation Methods in Eigenvalue Problems of Elastodynamics and Thin Plates* (Elsevier, Amsterdam, 1985).
[10] E. Dokumaci, "A Study of The Failure of Numerical Solutions in Boundary Element Analysis of Acoustic Radiation Problems," J. Sound Vib. 139, 83–97 (1990)
[11] B. Noble and J. W. Daniel, *Applied Linear Algebra* (Prentice-Hall, Englewood Cliffs, NJ, 1988).
[12] J. S. Arora, *Introduction to Optimum Design* (McGraw-Hill, New York, 1989).
[13] A. Craggs, "The Use of Simple Three-Dimensional Acoustic Finite Elements for Determining the Natural Modes and Frequencies of Complex Shaped Enclosures," J. Sound Vib. 23, 331–339 (1972).
[14] M. Petyt, J. Lea, and G. H. Koopmann, "A Finite Element Method for Determining the Acoustic Modes of Irregular Shaped Cavities," J. Sound Vib. 45, 495–502 (1976).
[15] R. K. Sigman and B. T. Zinn, "A Finite Element Approach for Predicting Nozzle Admittances," J. Sound Vib. 88, 117–131 (1983).
[16] M. L. Munjal, *Acoustics of Ducts and Mufflers* (Wiley, New York, 1987).